NURETH14-420

HEAT FLUX AND TEMPERATURE DETERMINATION ON THE CONTROL ROD OUTER SURFACE

J. Taler¹, A. Cebula¹, J. Marcinkiewicz², H. Tinoco²¹ Cracow University of Technology, Cracow, Poland
² Forsmarks Kraftgrupp AB, Östhammar, Sweden

Abstract

The paper presents heat transfer calculation results concerning a control rod of Unit 3 of Forsmark Nuclear Power Plant (NPP). The part of the control rod, which is the object of interest, is surrounded by a mixing region of hot and cold flows and, as a consequence, is subjected to thermal fluctuations. The paper describes a numerical test which validates the method based on the solution of the inverse heat conduction problem (IHCP). The comparison of the results achieved by two methods, CFD and IHCP, including a description of the IHCP method used in the calculation process, shows a very good agreement between the methods.

Introduction

For a few years ago, the occurrence of cracks due to thermal fatigue was detected in the control rods of Unit 3 of Forsmark NPP. As a part of an extensive damage investigation, time dependent CFD simulations were carried out, showing that the flow and heat transfer occurring within the annular region formed by the guide tube and control rod stem, are affected by large-scale perturbations coming from the upper warm water inlet (see Figure 1 and [1, 2]). Later, these CFD analyses were partially validated by experimental measurements of the flow conditions in the annular gap, but no measurements of the heat flux to the control rod were performed [3]. In the near future, an experiment will be run which will enable to estimate the heat flux through the rod outer surface using temperature measurements on the surface and within the rod. The estimation will be calculated by means of the methodology explained in the present work, which constitutes a proof of the correctness of the procedure when CFD temperature data are used instead of real temperature measurements. The objective of the experiment is to complete the validation of the CFD simulations by including heat flux measurements.

In this paper, heat transfer calculation results concerning the control rod simulated in [1, 2] are explained and reported. As mentioned before, the control rod is surrounded by a mixing region of hot and cold flows and, as a consequence, is subjected to thermal fluctuations. The determination of the unknown temperature and heat flux are based on measurements of the control rod temperature in some discrete points beneath the surface and does not require any knowledge of the fluid temperature field. This can be achieved by solving the inverse heat conduction problem (IHCP). The IHCP is defined as the estimation of the boundary conditions from transient temperature histories at one or more interior locations. Due to the ill-posedness of the IHCP, i.e. any small change on the input data can result in a dramatic change to the solution, it is more difficult to solve than the direct problem.

While waiting for the temperature measurements of the experiment, a test was started using the temperature time series of selected points extracted from the data set produced by the CFD simulations. With this temperature data, the heat flux was computed solving the IHCP and the results were compared with the corresponding of the CFD simulations. Each step of the test is explained in the following sections of this study.

Due to the symmetry of the boundary conditions, only a quarter of the rod is considered in the CFD model. Two levels on the rod height are investigated. Solid temperature histories in the discrete points located beneath the rod surface are used as the input data for the inverse analyses. "Measured" temperature histories are known from the CFD calculations. At each level 10 temperature "measurement" points are located. These points are distributed on two radiuses.

Due to the good agreement between the results obtained from the inverse procedure and those of the CFD simulations, the performed calculations support the usefulness of the proposed inverse method for the determination of rapid changes in temperature and heat flux on rod outer surface.

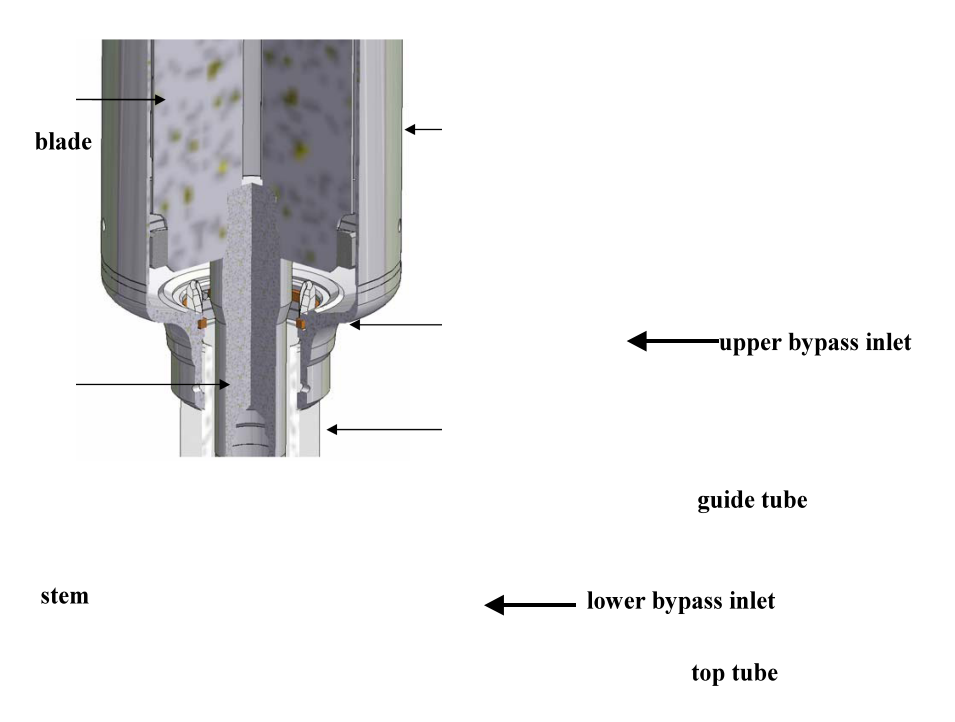


Figure 1 CAD-view of upper part of top tube with slip-on guide tube and control rod.

1. Discrete point location of the control rod

Determination of heat flux and temperature values is based on input data in discrete points of control rod. Two cross-sections are investigated; cross-sections are place on levels 1 and 2 as it is illustrated in Fig. 2. For level 2, the cross-section is a full solid but, for level 1, the cross-section has an annular shape with inner diameter $D_{in} = 40.0$ mm. The control rod outer diameter D_{out} is equal to 70.0 mm for both cross-sections. The distance between cross-sections placed on levels 1 and 2 is equal to 30.0 mm. Level 2 is 50.0 mm below the reference level, [1, 2].

To geometrically fit the CFD model with its symmetry boundary conditions, only one quadrant is considered. Temperature histories in discrete points, selected from CFD calculations performed by Forsmark Kraftgrupp, [1, 2], are used as the input data. There are 10 temperature points on

each level; the points are distributed on the radiuses: $R_1 = 25.0$ mm (points 1-5), and $R_2 = 34.5$ mm (points 6-10). There are 5 points on each radius with an angular spacing of 22.5°. Figure 3 shows the point distributions on cross-sections 1 and 2 respectively. Points 11-15 are placed on the outer rod surface, $R_{out} = 35.0$ mm, and in these points temperature and heat flux values are determined. Material properties implemented in the calculation procedure are temperature depended and correspond to material properties of austenitic stainless steel SS 2352.

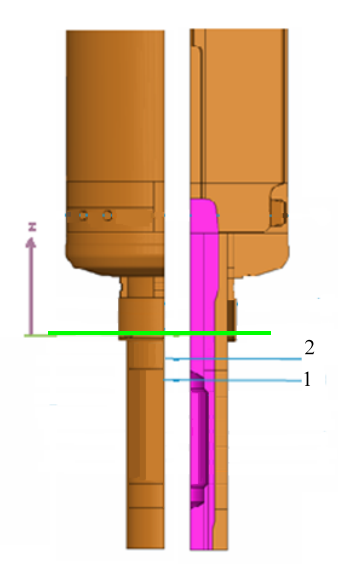


Figure 2 Location of planes 1 and 2 with input data. The green line represents reference level z = 0 situated in the center of the lower by-pass inlet.

2. Inverse heat conduction problem

The inverse heat conduction problem (IHCP) is defined as the estimation of the boundary conditions from transient temperature measurements at one or more interior locations. Due to the ill-posedness of the IHCP, it is more difficult to solve than the direct problem, [4, 5]. The method employed assumes that the temperature distribution on the surface S_m , which is located inside the analyzed area (see Fig. 4), is known. From the solution of the direct problem the heat flux density on the boundary S_m can be evaluated. Thus, the two conditions are known on the surface S_m :

$$T(S_m, t) = f(S_m, t), \tag{1}$$

$$-k\frac{\partial T}{\partial n}\Big|_{S_m} = q(S_m, t), \qquad (2)$$

while on the outer surface of the body S, the temperature and heat flux density are unknown. In order to evaluate the transient temperature distribution in the inverse region, this region is divided into control volumes. The method marches in space towards the outer surface of the body S by using the energy balance equations for the control volumes placed on the boundary

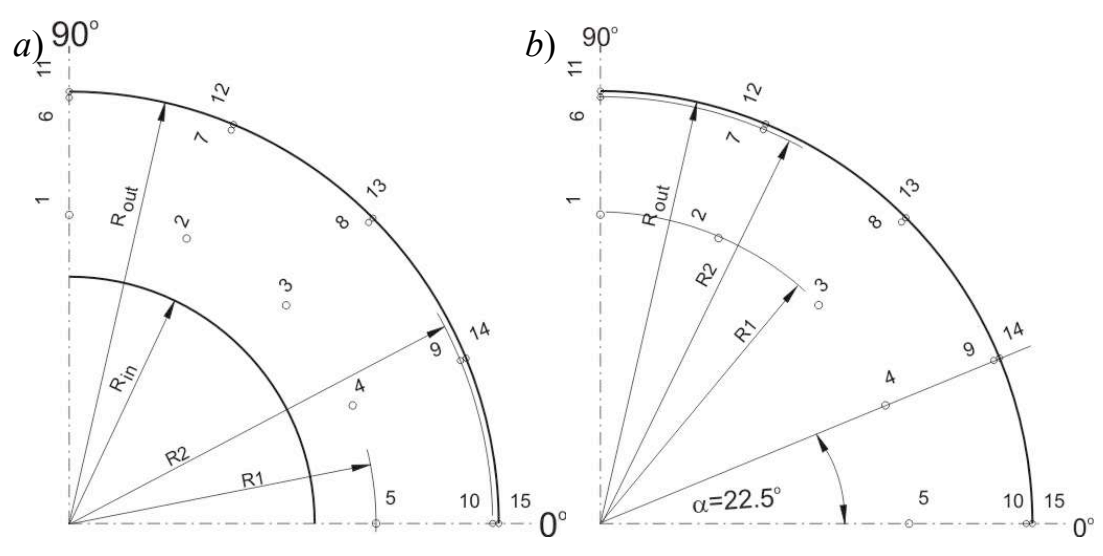


Figure 3 Characteristic points location: a) level 1; b) level 2.

 S_m to determine the temperatures in adjacent nodes. In order to further progress, the time derivatives of the "measured" temperature changes have to be calculated. Because the calculations of the time derivatives of the input temperature traces could be inaccurate due to incidental sampling errors, these time temperature sets have to be smoothed. In the present paper, the smoothing was achieved by using a local polynomial approximation. The consecutive 10 temperature data points were approximated using a polynomial of 3rd degree and then the derivatives in the middle of each interval were calculated, [6]. The spacemarching method will be illustrated by an example showing the evaluation of the temperature distribution in the control rod using the temperature input points equally distributed on radius r_5 (Fig. 5). It is assumed that the temperature and heat flux density distributions are known from direct solution in points 1-5(Fig. 5). The heat balance equations for the control volumes 8 yield:

$$c_{p}\rho \cdot \frac{\Delta\varphi}{2} \left(r_{4}^{2} - r_{2}^{2}\right) \frac{dT_{8}}{dt} = k \frac{T_{7} - T_{8}}{\Delta\varphi r_{3}} \cdot \Delta r + k \frac{T_{9} - T_{8}}{\Delta\varphi r_{3}} \cdot \Delta r + k \frac{T_{3} - T_{8}}{\Delta r} \cdot \Delta\varphi \cdot r_{2} + k \frac{T_{13} - T_{8}}{\Delta r} \cdot \Delta\varphi \cdot r_{4}, \quad (3)$$

where c_p is the specific isobaric heat capacity, ρ the density, k the thermal conductivity, with t as time and T as temperature. The temperature in node 13 is determine from equation (3) as

$$T_{13} = T_8 + \frac{\Delta r}{\Delta \varphi r_4 k} \left(c_p \rho \frac{\Delta \varphi}{2} \left(r_4^2 - r_2^2 \right) \frac{dT_8}{dt} - \left(k \frac{T_7 - T_8}{\Delta \varphi r_3} \Delta r + k \frac{T_9 - T_8}{\Delta \varphi r_3} \Delta r + k \frac{T_3 - T_8}{\Delta r} \Delta \varphi r_2 \right) \right). \tag{4}$$

Determining the temperature in nodes 12 and 14 in the same way and solving the balance equations for node 13 yields the equation for the heat flux density q_{13} :

$$q_{13} = \frac{1}{\Delta \varphi \cdot r_{5}} \left(\left(k \frac{T_{14} - T_{13}}{\Delta \varphi r_{5}} \cdot \frac{\Delta r}{2} + k \frac{T_{12} - T_{13}}{\Delta \varphi r_{5}} \cdot \frac{\Delta r}{2} + k \frac{T_{8} - T_{13}}{\Delta r} \Delta \varphi r_{4} \right) - c_{p} \rho \frac{\Delta \varphi}{2} \left(r_{5}^{2} - r_{4}^{2} \right) \frac{dT_{13}}{dt} \right). \quad (5)$$

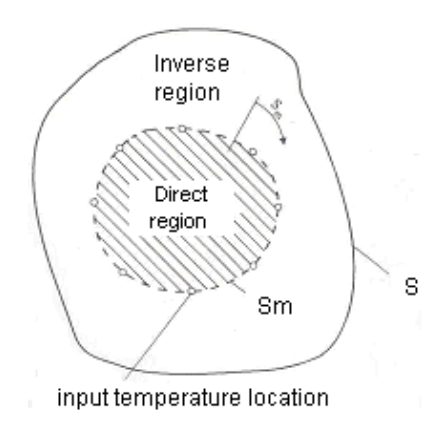


Figure 4 Two-dimensional inverse heat conduction problem, [6].

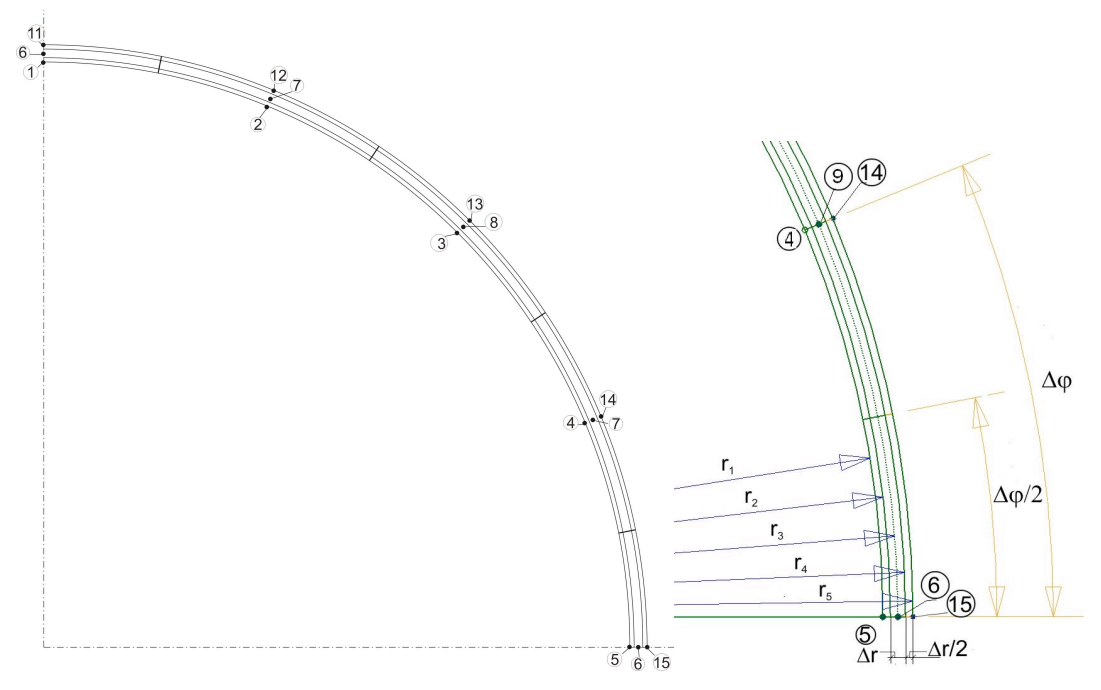


Figure 5 Part of the control rod wall divided into the control volumes, $r_5 = R_{out} = 35.0$ mm, $\Delta r = 0.5$ mm, $\Delta \varphi = 22.5^{\circ}$.

An inverse domain can be divided into non-regular or nonrectangular grids. If the body is irregularly shaped, then the developed method can also be used. In such a case, instead of applying the classical control volume method, the finite-element method should be used [5].

3. Input data

The flow simulations in the annular region between the top tube of the control rod drives and the control rod stem show a fairly irregular behavior of the turbulent flow within and above the mixing region between cold crud-cleaning and hot bypass flows. This mixing region is defined here as the zone that contains the strongest and most varying vertical temperature gradients. Below this mixing region, the flow is thermally stratified, stable, with low velocity and with a partially laminar part [1, 2]. Figure 6 shows a sequence of fluid temperature

distributions at the stem wall, where the time elapsed between views is approximately 7 to 8 seconds. Three horizontal planes are included, an upper plane located at the level of the lower bypass inlet, a midplane 100 mm below the upper plane and an lower plane 100 mm lower down. These views depict a relatively regular pattern change of the temperature distribution that seems to have a period of about 15 seconds. The pattern change from one side to the other takes place in about 2 to 2.5 seconds which shows that the process is rather abrupt. The related animation of the temperature distribution shows as well the presence of many small and intermediate scale temperature fluctuations of the mixing region having frequencies of the order of 1 Hz or higher, [1].

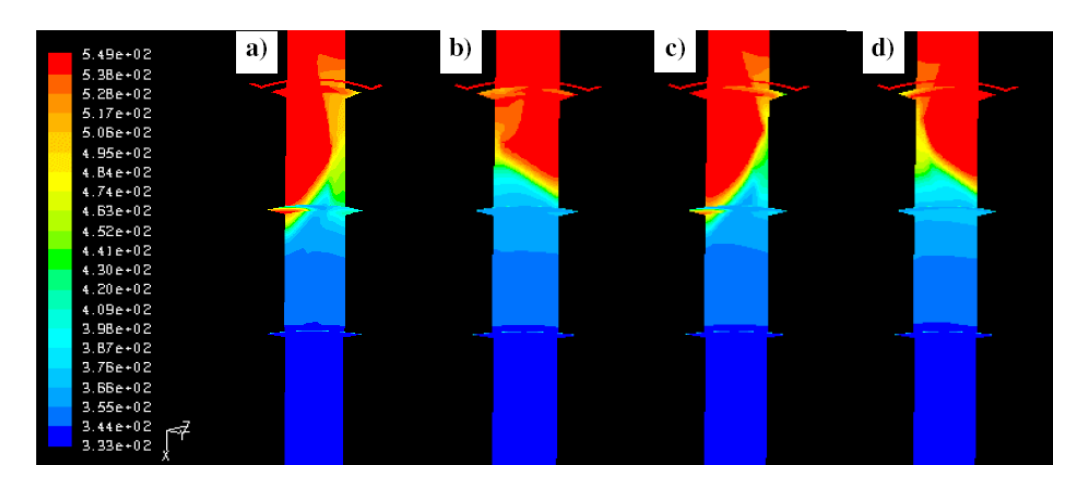


Figure 6 Sequence of fluid temperature distributions (in K) at the stem wall: a) view at arbitrary time equal 0 s; b) at 7.15 s; c) at 14 s; d) at 22.35 s [1].

The sequence of temperature distributions given by Fig. 6 indicates that low frequencies seem to be included in the spectrum of the temperature fluctuations that affect the surface of the outer wall of the stem. As an example, Figure 7 shows the time signal of the temperature for three points located in the middle of the mixing region and along a radial line. The green curve corresponds to the signal of a point in the fluid close to the stem wall, the red corresponds to the signal of a point in the stem at the outer wall and the blue corresponds to the signal of a point a few millimeters inside the stem. The signals in the stem have lower amplitude with slower oscillations due to the properties of the solid material. Most of the energy of the spectrum is concentrated to frequencies lower than 0.1 Hz for all three points. For the point in the fluid as well for the point at the solid surface there are two maxima in this range of frequencies while for the point inside the solid there is only one maximum at the lowest frequency of approximately 0.02 Hz (Fig.8). This result agrees well with the properties of the material of the stem, i.e. only slow fluctuations of the temperature can penetrate the solid. Two levels of the control rod have been considered in this work. For each level, 10 points were chosen, with their position depicted in Fig. 3. CFD calculations allow to generate temperature time series. Such data were prepared for the considered levels and introduced as input to developed mathematical model based on the solution of the IHCP. Examples of input temperature histories are presented in Figures 9 and 10. These figures present solid temperature histories inside the stem for several angular values. These figures show high temperature oscillations for points located close to the outer surface (blue lines). However, as the distance from outer surface increases, the temperature oscillations

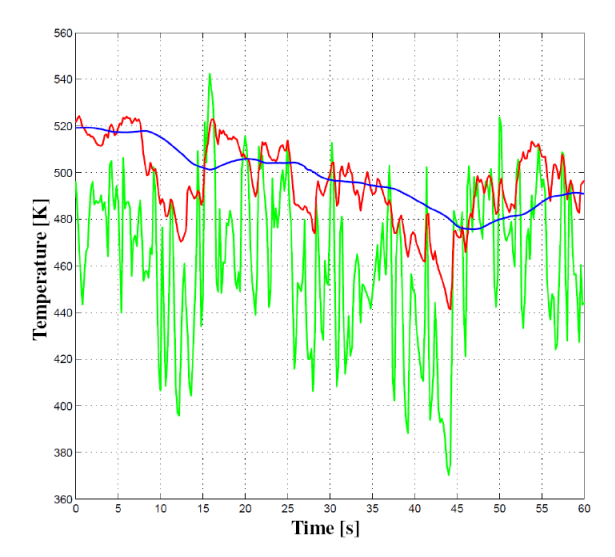


Figure 7 Time signal of temperature, in K, for three points at the center of the mixing region, along a radial line; point in fluid (green), points in solid (red and blue).

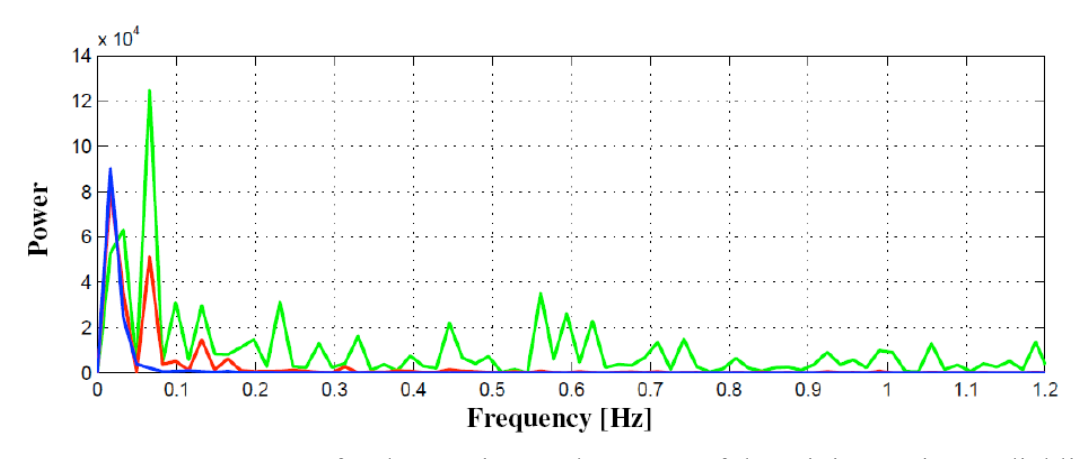


Figure 8 Frequency spectrum for three points at the center of the mixing region, radial line; point in fluid (green), points in solid (red and blue).

are noticeably damped. Red lines represent temperature histories for points located 10 mm underneath the outer surface. From the analysis of the input data follows that the range of variation of the solid temperature is between 132 °C and 213 °C for level 1 and between 171 °C and 240 °C for level 2.

4. Smoothing the temperature data

The solution of the IHCP depends on the solid temperature and time derivatives of temperature. The IHPC is ill-posed. Therefore, the solutions are very sensitive to errors in input data. Variations in the surface conditions of the body are attenuated at interior locations of the body. Conversely, the small errors in the input data are magnified at the surface and may cause large oscillations in the estimated surface temperature and heat flux, [6]. To minimize the effects of noisy data, the temperature should be smoothed before they are used in the IHCP algorithm. If the temperature data are corrupted with random errors, least squares smoothing may be used to reduce the effect of the errors on the calculated time derivatives dT_i/dt .

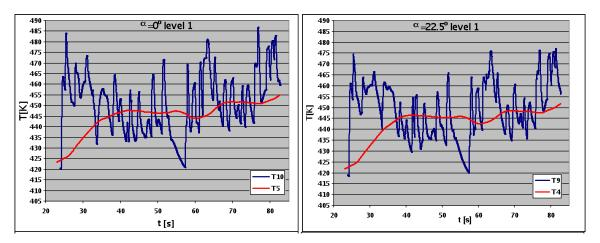


Figure 9 Input temperature histories for level 1 for radius $R_1 = 25.0$ mm and $R_2 = 34.5$ mm and angular positions a) 0° , b) 22.5°

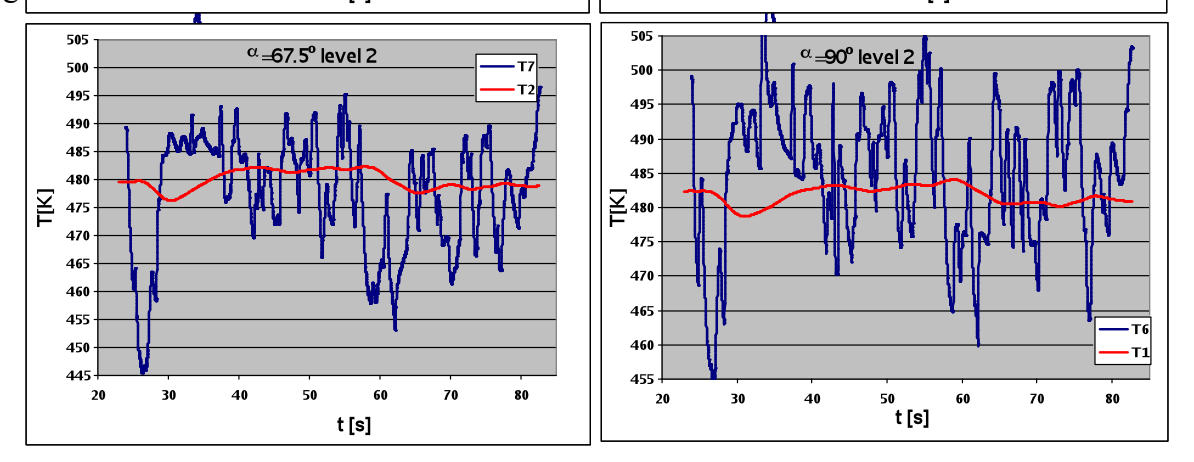


Figure 10 Input temperature histories for level 2 for radius $R_1 = 25.0$ mm and $R_2 = 34.0$ mm and angular positions a) 67.5° , b) 90°

Least squares approximation is indeed very suitable for the recovery of a smooth function from noisy information. It is possible to choose an appropriate function which is flexible enough to reconstruct the underlying noise free function and its derivative while still orthogonal to the noise, i.e. unable to follow the oscillations in the data. Here, the Gram orthogonal polynomials will be used for smoothing the time-temperature history f(t) and estimated temperatures T_i . Piecewise cubic polynomials are constructed and then used in a least square procedure to estimate appropriate polynomial coefficients. The temperature f(t) is given with equal time steps Δt for $N_t = (2L+1)$ successive time points $t_j = (j-1) \Delta t$, $j = 1, ..., N_t$ and the local Gram polynomial is constructed. Introducing a new dimensionless time coordinate (Fig. 11)

$$s = \frac{t_j - t_i}{\Delta t} - L \,, \tag{6}$$

the coefficients of the Gram polynomial y(s) are determined using the least squares method

$$\sum_{s=-L}^{s=L} \left[y(s) - f(s) \right]^2 = \min. \tag{7}$$

The coefficients of the polynomial y(s) are obtained from normal equations. A third order polynomial for the set of N = 9 data points is

$$y(s) = \frac{1}{9} (f_{-4} + f_{-3} + f_{-2} + f_{-1} + f_0 + f_1 + f_2 + f_3 + f_4) +$$

$$+ \frac{1}{15} \left(-f_{-4} - \frac{3}{4} f_{-3} - \frac{1}{2} f_{-2} - \frac{1}{4} f_{-1} + \frac{1}{4} f_1 + \frac{1}{2} f_2 + \frac{3}{4} f_3 + f_4 \right) s +$$

$$+ \frac{1}{99} \left(f_{-4} + \frac{1}{4} f_{-3} - \frac{2}{7} f_{-2} - \frac{17}{28} f_{-1} - \frac{5}{7} f_0 - \frac{17}{28} f_1 - \frac{2}{7} f_2 + \frac{1}{4} f_3 + f_4 \right) (3s^2 - 20) +$$

$$+ \frac{7}{2970} \left(-f_{-4} + \frac{1}{2} f_{-3} + \frac{13}{14} f_{-2} + \frac{9}{14} f_{-1} - \frac{9}{14} f_1 - \frac{13}{14} f_2 - \frac{1}{2} f_1 + f_4 \right) (5s^2 - 59s),$$

$$(8)$$

where s = -4,...,0,...,4.

Differentiating the equation above with respect to t yields:

$$\frac{dy}{dt} = \frac{1}{\Delta t} \frac{dy(s)}{ds} = \frac{1}{\Delta t} \left[\frac{1}{15} \left(-f_{-4} - \frac{3}{4} f_{-3} - \frac{1}{2} f_{-2} - \frac{1}{4} f_{-1} + \frac{1}{4} f_{1} + \frac{1}{2} f_{2} + \frac{3}{4} f_{3} + f_{4} \right) + \frac{2}{33} \left(f_{-4} + \frac{1}{4} f_{-3} - \frac{2}{7} f_{-2} - \frac{17}{28} f_{-1} - \frac{5}{7} f_{0} - \frac{17}{28} f_{1} - \frac{2}{7} f_{2} + \frac{1}{4} f_{3} + f_{4} \right) s + \frac{7}{2970} \left(-f_{-4} + \frac{1}{2} f_{-3} + \frac{13}{14} f_{-2} + \frac{9}{14} f_{-1} - \frac{9}{14} f_{1} - \frac{13}{14} f_{2} - \frac{1}{2} f_{1} + f_{4} \right) \left(5s^{2} - 59 \right) \right], \tag{9}$$

where s = -4,...,0,...,4.

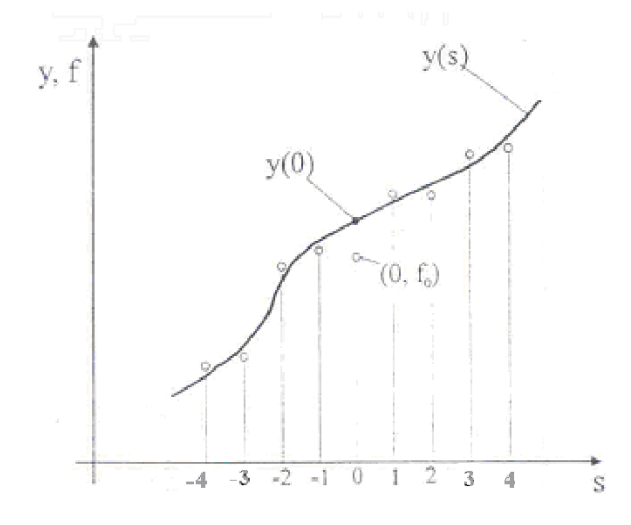


Figure 11 Time smoothing of the temperature using N=9 point averaging filter.

The smoothed temperature and its time derivative are evaluated at the center point t (s = 0). Future and past data appear in equations (8) and (9), where the points s = 1, ..., 4 are the future data and s = -1, ..., -4 are the past data. Having calculated the temperature and its time derivative at the center point t (s = 0), the whole time interval $8 \cdot \Delta t$ is moved one time step forward, dropping the last data point s = -4 and adding a new one. When the real process begins, no past data are available. Due to complexity of the formulas for the first and last four time points, calculations for theses points are dropped.

5. Results

Results from CFD calculations are used as the input data to develop a mathematical model based on the inverse method. The aim of the developed model is to calculate temperature and heat flux on the stem outer surface. The determined outer temperatures at points 15, 14 for level 1 and 2 are presented in Figures 12 and 13. In addition to the surface temperatures, solid temperatures for points with a depth of 0.5 mm are also depicted. From the analysis of the results, it possible to observe that the surface temperature may have higher values than the corresponding at a point slightly under the surface during the stage of temperature rise and opposite situation can be noticed during the stage of the temperature decrease. Such distinctive temperature results are consistent both with physics and the expectations of the methodology.

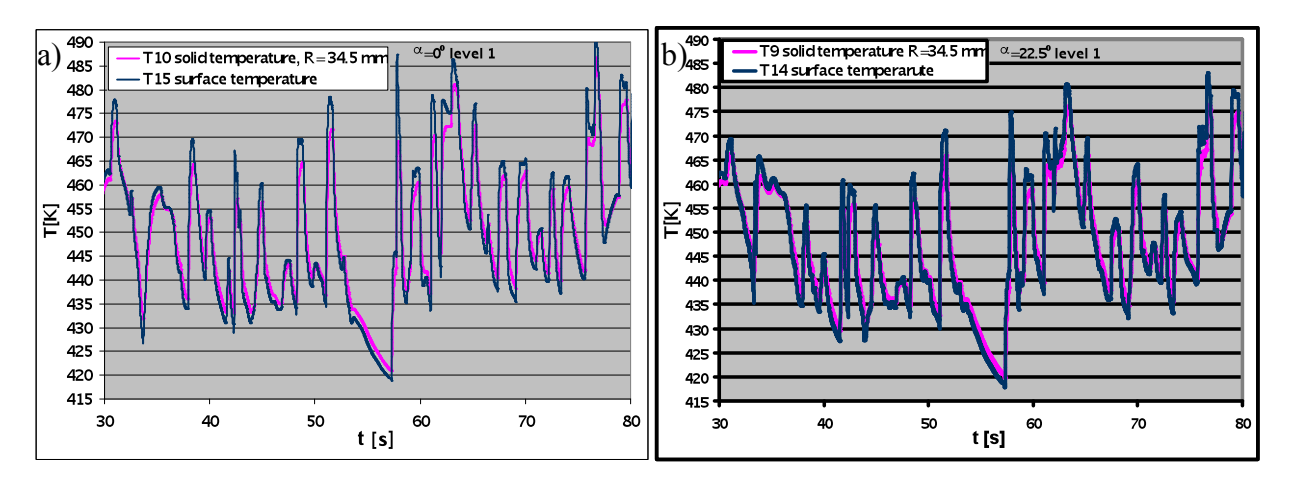


Figure 12 Surface temperature from the IHCP solution and solid temperature histories, level 1: a) point 10 and 15, angle 0° b) point 9 and 14, angle 22.5°

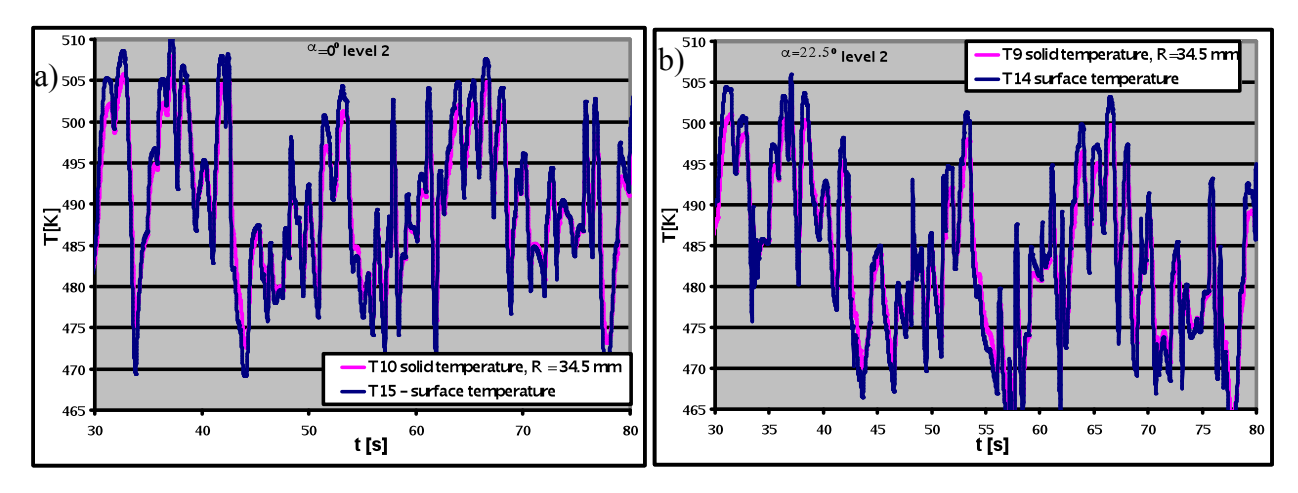


Figure 13 Surface temperature from the IHCP solution and solid temperature histories, level 2: a) point 10 and 15, angle 0 ° b) point 9 and 14, angle 22.5°

The determined heat flux values for points 11 and 12 are presented in Figures 14 and 15. The heat flux values range from $18.9 \cdot 10^5$ W/m² to $-6.2 \cdot 10^5$ W/m² at level 1 and from $9.3 \cdot 10^5$ W/m² to $-6.6 \cdot 10^5$ W/m² at level 2.

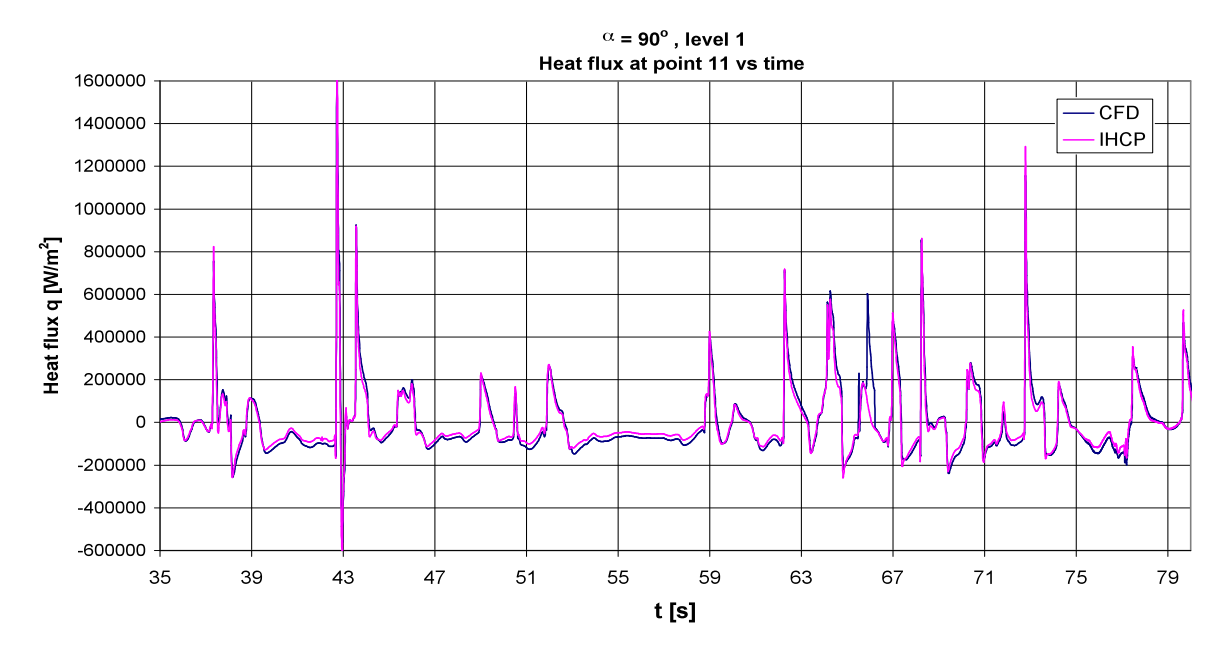


Figure 14 Surface heat fluxes from CFD and IHCP method at point 11, level 1.

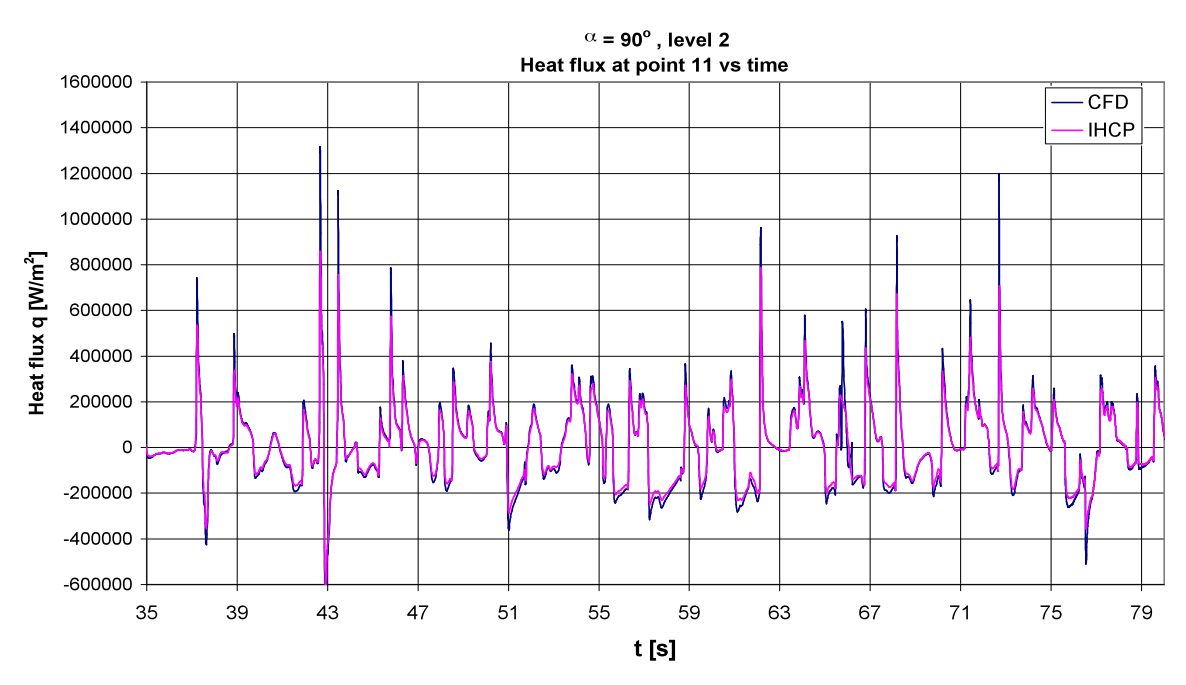


Figure 15 Surface heat fluxes from CFD and IHCP method at point 11, level 2.

The calculation results (Fig. 16) show that rapid outer surface temperature variations correspond to rapid changes in heat flux. Maximum values of heat flux appear before maximum values of temperature. The analysis also demonstrates that constant heat flux values are obtained when temperature increases or decreases at a constant rate.

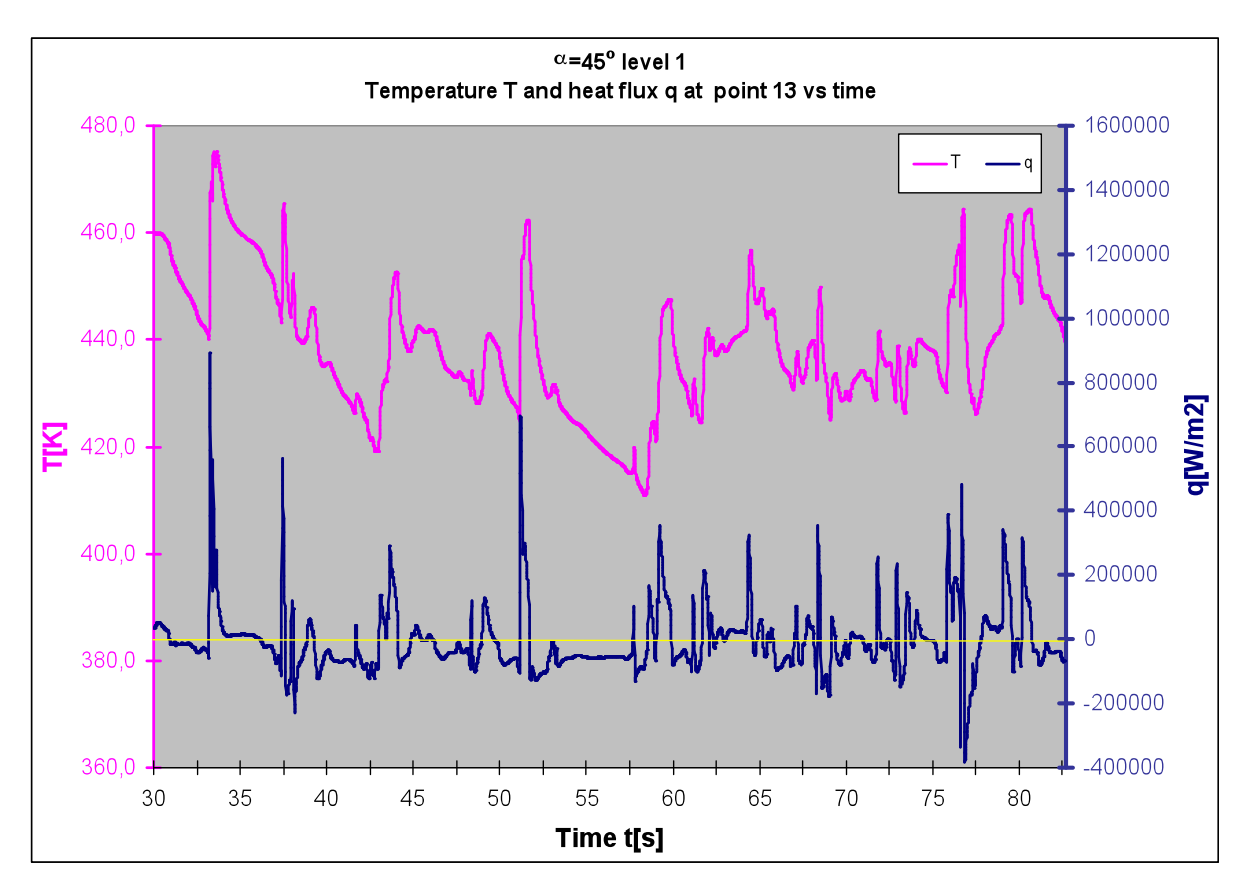


Figure 16 Time temperature T and heat flux q histories obtained from the IHCP solution at point 13 – level 1.

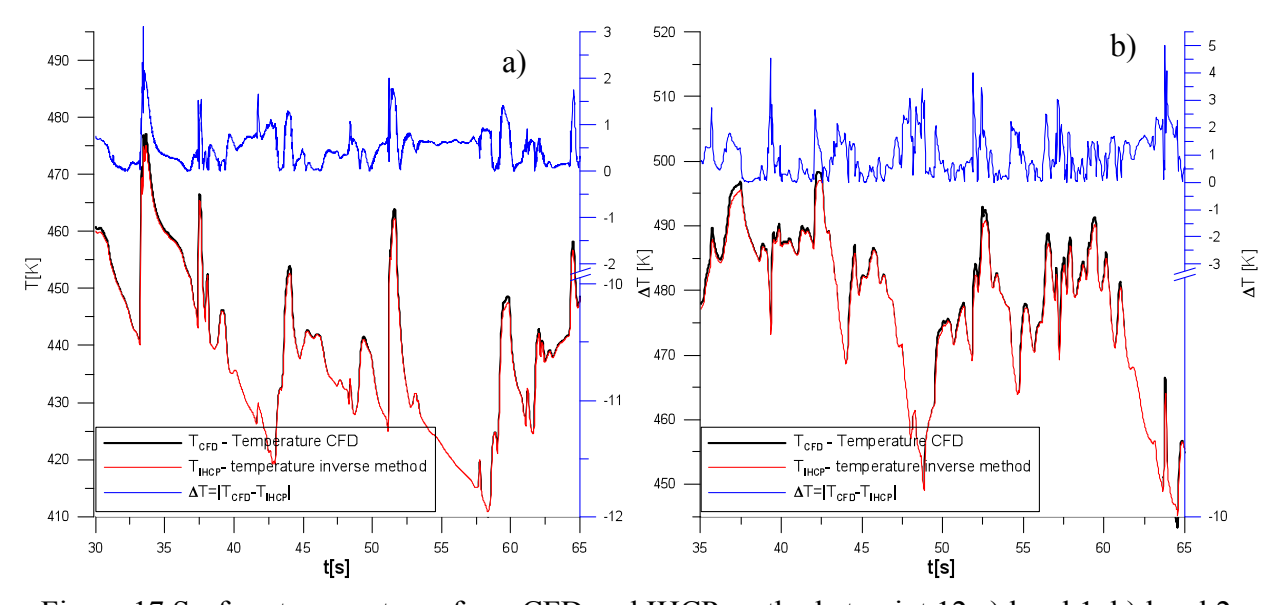


Figure 17 Surface temperatures from CFD and IHCP method at point 12 a) level 1, b) level 2.

During the rise of the outer surface temperature, the heat flux also rises and may reach high positive values. It represents a heat inflow through the rod surface. When the converse occurs, i.e. during temperature decrease, the heat flux also decreases and may reach low negative values. Negative values indicate that the element is locally cooled and the flux is reversed, i.e. heat flows out of the control rod into the fluid.

Also a comparison between CFD results and the IHCP method results has been carried out. Examples of this comparison for point 12 for both levels are presented in Figure 17. The black line corresponds to surface temperature from CFD calculations and the red corresponds to surface temperature from the IHCP method. The comparison reveals a quite good agreement between results and, for particular time periods, the curves overlay each other. The blue line in Figure 17 represents the temperature difference $\Delta T = |T_{\text{CFD}} - T_{\text{IHCP}}|$ between the methods that corresponds to the ordinate scale to the right in the figure. The average difference amounts to 1.5 K. The largest difference values appear in regions of high temperature amplitudes. The comparison analysis of surface heat fluxes establishes a very good agreement between the results obtained with the two methods. The heat flux comparison for point 11 is illustrated in figures 14 and 15 for level 1 and 2, respectively. It may be concluded that the developed IHCP method reconstructs heat flux histories well.

6. Conclusions

The calculation results reported in this work confirm the possibility of reconstructing rapid surface heat flux and temperature changes occurring at the surface of a solid body with the presented IHCP method. The numerical verification shows that the obtained results using the IHCP method are in good agreement with the results of CFD simulations.

It must be emphasized that the method does not require the analyst to set boundary conditions concerning the fluid since the temperature information corresponding to a finite number of points inside the solid body is needed. This property of the method constitutes a great advantage for defining the characteristics of the conjugate heat transfer when the flow conditions are highly transient, as is the case with the control rod. In this case, the heat flux at the solid surface varies strongly and no reasonable temperature difference between solid and fluid may be defined, rendering a realistic determination of a heat transfer coefficient practically impossible. The fact that transient heat fluxes might be measured accurately using the IHCP method, a prospect that will be confirmed in the planned future experiments, unfolds the possibility of defining heat transfer correlations based directly on this magnitude rather than on the steady concept constituted by the heat transfer coefficient.

Nomenclature

```
c_p — specific heat, J/(kg·K)
D_{\text{in}} — inner diameter, m
D_{\text{out}} — outer diameter, m
f — measured ith temperature, °C
k — thermal conductivity, W/(m·K)
N_t = (2L+1) — number of input data points in moving average filter q — heat flux, W/m²
R_{\text{in}} — inner radius, m
R_{\text{out}} — outer radius, m
```

The 14th International Topical Meeting on Nuclear Reactor Thermalhydraulics, NURETH-14 Toronto, Ontario, Canada, September 25-30, 2011

r — radius, m s — dimensionless time coordinate S — surface

T – temperature, °C

t – time, s

 $\Delta \varphi$ – control volume size in tangential direction, rad

 Δr – control volume size in radial direction, m

 Δt – time step, s ρ – density, kg/m³

References

- [1] H. Tinoco and H. Lindqvist, "Thermal Mixing Instability of the flow inside a control-rod guide tube", <u>Proceedings of NURETH-13</u>, Japan, Kanazawa 2009.
- [2] H. Tinoco, H. Lindqvist, Y. Odemark, C.-M. Högström, B. Hemström & K. Angele, "Flow Mixing Inside a Control-Rod Guide Tube Part I: CFD Simulations", <u>Proceeding of the 18th International Conference on Nuclear Engineering (ICONE 18)</u>, Xi'an, China, 2010 May 17-21.
- [3] K. Angele, M. Cehlin, C.-M. Högström, Y. Odemark, M. Henriksson, H. Tinoco & H. Lindqvist, "Flow Mixing Inside a Control-Rod Guide Tube Part II: Experimental Tests and CFD-Validation", <u>Proceeding of the 18th International Conference on Nuclear Engineering (ICONE 18)</u>, Xi'an, China, 2010 May 17-21.
- [4] J. Taler, B. Węglowski, W. Zima, S. Grądziel, M. Zborowski, "Analysis of thermal stresses in boiler drum during the start-up", Transaction of the ASME, Vol. 121, 1999
- [5] J.Taler and P. Duda, "Solving direct and inverse heat conduction problems", Springer, 2006
- [6] J. Taler, W. Zima "Solution of inverse heat conduction problem using control volume approach", Int. J. of Heat and Mass Transfer, 43, 1999.
- [7] J. Taler, B. Węglowski, W. Zima, S. Grądziel, M. Zborowski, "Monitoring of transient temperature and thermal stresses in pressure components of steam boilers", Int. J. Pres. Ves. & Piping, 72, 1997, pp. 231-241.